# Direct Observation of Right and Left Helical Hands of Syndiotactic Polypropylene by Atomic Force Microscopy

**W. Stocker,† M. Schumacher, S. Graff, J. Lang, J. C. Wittmann, A. J. Lovinger,*,‡ and B. Lotz***

*Institut Charles Sadron (CRM-EAHP), CNRS and ULP, 6, rue Boussingault, 67083 Strasbourg Cédex, France, and AT&T Bell Laboratories, 600 Mountain Avenue, Murray Hill, New Jersey 07974*

*Received March 31, 1994*®

ABSTRACT: Syndiotactic polypropylene (sPP), epitaxially crystallized on *p*-ter- or *p*-quaterphenyl is investigated by electron microscopy and diffraction and atomic force microscopy (AFM). The epitaxial relationship between the *bc* contact face of sPP and the substrate (001) plane is established. In the *bc* contact plane, the sPP helices display a succession of $CH_3$, $CH_2$, and $CH_3$ groups tilted at 45° to the helical axes. These groups have been visualized by AFM in a liquid cell, thus providing the first direct observation, in unfiltered images, of arrays of *both* right and left hands of individual polyolefin helices embedded in their crystallographic environments.

## Introduction

Helical hand is a central issue in the crystal structure analysis of syndiotactic polypropylene (sPP), as it governs the cell symmetry and is at the root of a specific type of crystal structure defect. The molecular conformation established by Corradini et al.[1] for sPP is of the type $(t_2g_2)_2$ and results in an s(2/1)2 helix with a *c* axis repeat of 0.74 nm. The unit cell first proposed is orthorhombic with parameters $a$ = 1.45 nm, $b$ = 0.560 nm, and $c$ = 0.74 nm, space group $C222_1$. It is a C-centered cell (in chain axis projection) in which helices have the same hand (either all left or all right) (Figure 1a).[1] More recent work showed that the stable crystal structure of solution-grown crystals and bulk-crystallized material has a unit cell (cell III[2,3]) with a *b* parameter doubled to 1.12 nm and involves a different chain packing (Figure 1b). The root of this crystal polymorphism lies in the hand of constituting helices. The new cell implies strict alternation of right- and left-handed helices along both *a* and *b* axes, resulting in a highly symmetrical space group (*Ibca*, with 16 monomers in the unit cell).[2] Further, a structural disorder becomes more and more prominent as the crystallization temperature decreases.[3] It results from *b*/4 shifts of sPP layers, which are produced by "mistakes" in the alternation of helical hands in the *bc* plane and may be thought of as the progressive intrusion of the initial C-centered packing scheme as a defect into the more stable one. The faults are revealed by specific streaks in the *hk*0 diffraction patterns of single crystals and are due to empty crystallographic sites of size equivalent to half a helix (i.e. 0.28 nm) along the *b* axis direction which lead to displaced rows or stacking faults. All these effects are well documented and have been analyzed[4] by molecular modeling and optical masks. The impact on the diffraction pattern of these and other possible defects has also been evalulated recently.[4–6]

As is apparent from molecular models (Figure 2), the helical hand of sPP molecules is particularly prominent in the *bc* plane. In fact, in this plane, the $CH_2$ group with gg conformation and the two nearby methyl side chains

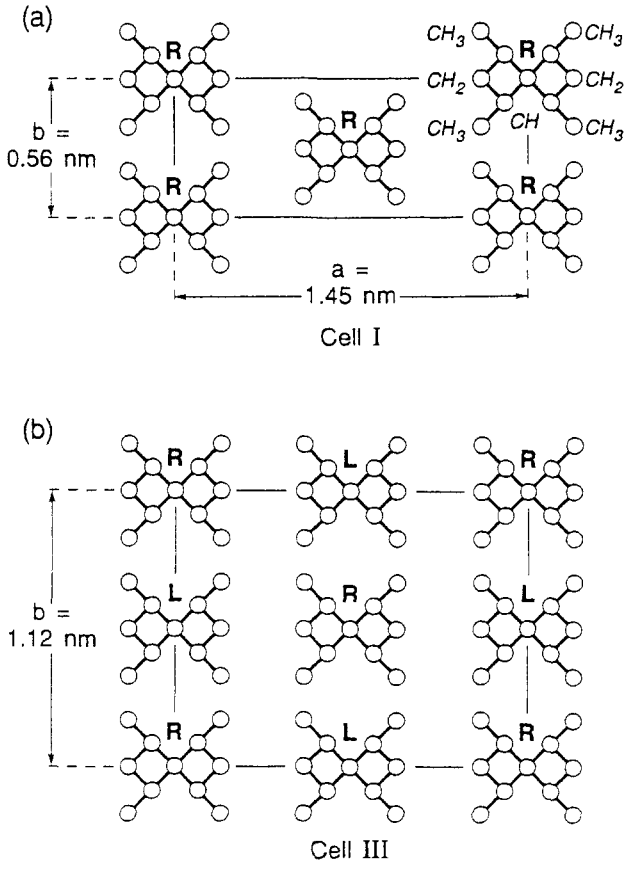


**Figure 1.** Two unit cells proposed for the stable form of syndiotactic polypropylene, as shown in the *c* axis projection: (a) C-centered cell I with isochiral chains; (b) body-centered cell III with alternation of right (R) and left (L) helical hands along both *a* and *b* axes.

are exposed on the molecular envelope. Taken together, they mimic an *n*-pentane molecule in all-trans conformation that is observed parallel to the C—C—C bonds plane. These molecular segments are inclined at 45° to the helix axis. As a result, exposed stretches of right- and left-handed helices are oriented nearly at right angles to each other (Figure 2).

The *bc* face of sPP appears well suited for examination by atomic force microscopy (AFM). When applied to suitable polymeric materials, AFM has indeed reached methyl group resolution, as illustrated, among others, by the visualization of end groups and fold structure in crystals of linear and cyclic paraffins,[7] of chain structure in thin

* To whom correspondence should be addressed.
† Present address: Johannes Gutenberg Universität Mainz, Institut für Physikalische Chemie, Jakob Welder Weg 11, D-55099 Mainz, Germany.
‡ AT&T-Bell Laboratories, 600 Mountain Ave., Murray Hill, NJ 07974.
® Abstract published in *Advance ACS Abstracts*, September 1, 1994.

0024-9297/94/2227-6948$04.50/0 

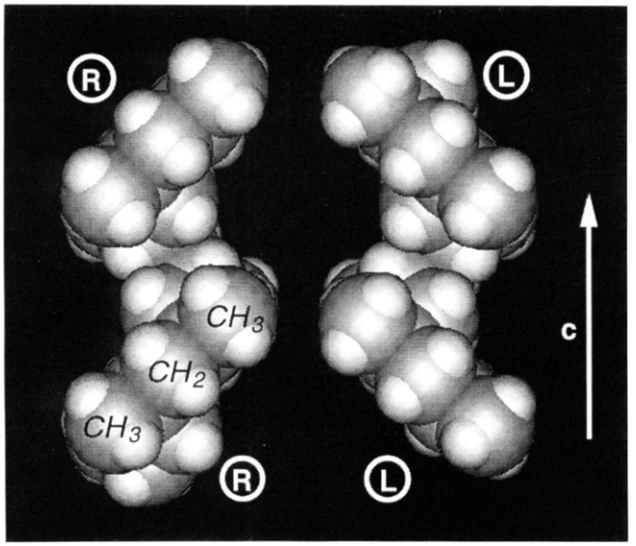


**Figure 2.** Computer-generated molecular models of right- and left-handed sPP helices in $(t_2g_2)_2$ conformation, as seen along the crystallographic *a* axis (left and right hand sides of the figure, respectively). Note the prominent rows of $CH_3$, $CH_2$, and $CH_3$ groups at 45° to the chain axis direction, which reveal unambiguously the helical hand.

films of rubbed PTFE[8-11] and poly(oxymethylene),[12] and of the pattern of methyl groups in isotactic polypropylene either epitaxially crystallized[13] or stretched.[14]

In the present investigation, we describe the epitaxial crystallization of sPP on suitable organic substrates which makes it possible, after dissolution of the substrate, to expose the sPP *bc* plane of interest. The film structure was investigated by transmission electron microscopy (TEM) and electron diffraction (ED). The exposed face was examined by AFM, which, as will be shown, does indeed reveal the hand of individual helices on that face. A more ambitious objective was also to visualize the above mentioned isochiral packing defects which, from earlier modeling of defective structures, are known to be quite rare.[4] This second, more elusive, objective has not yet been achieved.

Finally, epitaxially crystallized sPP investigated here by AFM is used in the companion paper to analyze a polymer–polymer epitaxy between sPP and polyethylene and a case of a rotation twin or epitaxy of sPP onto itself (homoepitaxy).[15]

## Experimental Section

**Materials.** Two syndiotactic polypropylenes of different origins were used in the present investigation: a highly syndiotactic material kindly provided by Dr. T. Simonazzi of Himont, Novara, Italy (>99% racemic diads), and a slightly less stereoregular polymer (ca. 93% racemic diads) provided by Exxon Chemical International (Dr. P. Agarwal). Except for well-documented shifts in melting temperatures linked with the different stereoregularities, no significant difference in behavior and/or crystal morphology could be detected: the discussion will therefore not include the specific polymer used.

The organic substrates are *p*-quaterphenyl (4Ph) and *p*-terphenyl (3Ph) of commercial origin (Fluka), used without further purification.

**Sample Preparation.** The crystallization procedure involved several steps.[16] A thin film of sPP was deposited onto a glass cover slide by evaporation at ~140 °C of a dilute solution (0.1% w/v) of the polymer in *p*-xylene. Single crystals of *p*-ter- or *p*-quaterphenyl were produced independently by slow cooling of a *p*-xylene solution from its boiling temperature; a drop of the suspension was deposited onto the polymer film at room temperature, leaving, after evaporation of the solvent, large (~10–50 μm), flat crystals of the oligophenyl scattered on top of the polymer film. This composite material was heated to ~160 °C to melt the sPP, but only for a short time in order to limit sublimation of the oligophenyl substrate, and then recrystallized by cooling at a controlled rate (−20 °C/min). At that stage, sPP crystallized epitaxially on the oligophenyl crystals. Note that since the oligophenyl acts in this epitaxial crystallization as a *substrate*, it will be referred to in the following as such, in spite of the fact that, in the actual crystallization procedure, it lies on top of the molten polymer film. The oligophenyl substrate crystals were subsequently dissolved away with hot amyl acetate. The films were left overnight under primary vacuum to further remove possible traces of the substrate by sublimation. The original substrate crystal position was still detectable by the imprint of its external contour in the sPP film, but the polymer contact face was now exposed.

**Electron Microscopy.** The thin sPP film was, if desired, shadowed with Pt/C, then backed with a carbon film, floated off on water with the help of a poly(acrylic acid) backing, and mounted on copper grids before examination in transmission and selected area diffraction modes in a Philips CM12 electron microscope equipped with a rotation–tilt stage.

**Atomic Force Microscopy.** AFM experiments were carried out with a Nanoscope III microscope (Digital Instruments, Inc., Santa Barbara, CA) where the deflection (*z* direction) of the tip is followed by that of a laser beam reflected on the rear side of the cantilever. The AFM pictures were obtained with an A-type scan head (maximum scan range: 700 × 700 nm²). $Si_3N_4$ tips attached to a microfabricated cantilever (200 μm, triangular base) were used. The force constant of the cantilever is small: 0.06 N/m. For distance calibration of the piezo controller, images of mica and highly oriented pyrolytic graphite (HOPG) were employed.

After removal of the oligophenyl substrate, the sPP samples prepared on glass coverslides were ready for examination by AFM. They were installed on the Nanoscope stage with the help of an optical microscope: the tip was positioned close to the surface of preselected flat regions of the film, which are easily identified by the imprints left by the (by now dissolved) substrate crystals. Scanning line frequencies were 1 Hz for large-scale scans (when imaging the lamellar structure) and up to 57 Hz for atomic resolution. Images presented here are preferably raw data (unless otherwise stated) to avoid filtering-induced bias of the morphology. For determination of lattice parameters of periodic structures, two-dimensional fast Fourier transform (2D-FFT) is applied on the raw, unfiltered data images.

AFM imaging in a liquid environment yields much improved resolution since reduction of capillary forces makes it possible to use imaging forces on the surface nearly 10 times smaller than in air. Imaging in a liquid environment is performed with the "liquid cell" limited on the top by the Plexiglas of the cantilever holder and on the bottom by the sample, whereas the side is sealed by an O-ring (for more details, see the paper by Drake et al.[17]). Water was chosen as a medium for imaging, on the basis of previous results and trial runs in air, methanol, and benzyl alcohol. Stable imaging was possible within a few minutes after adding the liquid. All three liquids yield similar quality pictures, although mainly those obtained with water are presented here.

**Molecular Modeling.** Molecular modeling was performed on a Silicon Graphics computer system using the Cerius molecular modeling software package for materials research (Molecular Simulations, Inc. of Burlington, MA, and Cambridge, U.K.).

## Results

**1. Electron Microscopy: Epitaxial Relationship between sPP and Linear Oligophenyls and the Structure of the sPP Films.** *The lamellar morphology* of epitaxially crystallized sPP is shown in Figure 3. Lamellae are edge-on, as is usually observed in polymer epitaxy.[16] The lamellar thickness is in the 15 nm range. Only one main lamellar orientation is present, parallel to the short diagonal of the lozenge-shaped substrate crystal, whereas epitaxy of polyethylene on the same substrates results in two different lamellar orientations, at ~70° to each other.[18] From the known 3Ph and 4Ph crystal

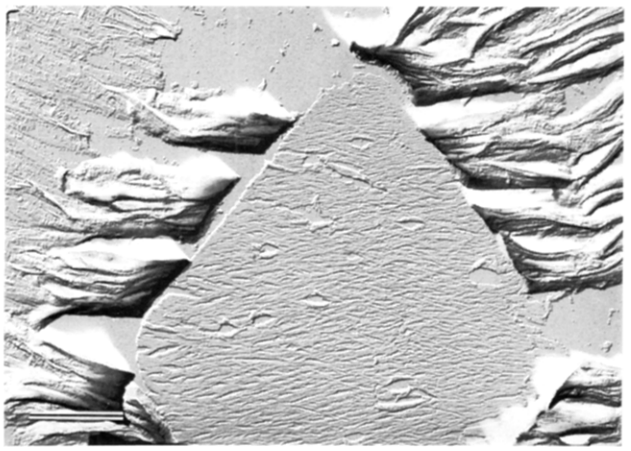

**Figure 3.** Lamellar morphology of sPP epitaxially crystallized on the (001) face of a *p*-terphenyl crystal. Note the general orientation of the lamellae parallel to the short diagonal of the substrate crystal and the imprint left by the latter, which helps to locate areas of interest for AFM. Electron micrograph, Pt—C shadowed at $\tan^{-1} = {}^1/_3$, scale bar = 2 $\mu$m.

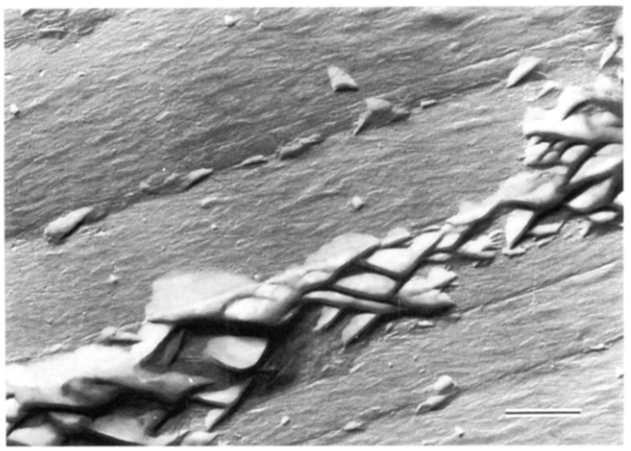

**Figure 4.** Other epitaxially crystallized sPP film with lamellae growing "inside" the *p*-terphenyl substrate. Note the much exaggerated angle of the lamellar planes as compared to the background lamellae. Electron micrograph, Pt—C shadowed at $\tan^{-1} = {}^1/_3$, scale bar = 2 $\mu$m.

parameters and growth morphology (cf. ref 18), the sPP lamellae lie on the large (001) substrate plane and are parallel to its *b* direction, which implies that the sPP chain axis is parallel to the substrate *a* axis.

Within this general picture, variations of ±10° of lamellar orientation are observable, resulting in a characteristic "corrugated" appearance of the morphology. Such orientations appear to reflect initial local superficial dissolution of the substrate crystal in the molten sPP, as better indicated by occasionally more prominent growth features illustrated in Figure 4. In this figure, sPP growth resulted in significant protrusions above the surrounding film; i.e. growth occurred toward and inside the substrate 3Ph crystal. In this area, local dissolution of 3Ph was followed by cocrystallization of 3Ph and sPP, most probably as a eutectic. Interestingly, in the resulting cellulated growth, the shape of the (by now missing) 3Ph crystals reproduces the angles between sPP lamellae observed in Figure 3. The latter angles appear therefore as substrate- or rather eutectic-induced (and not intrinsic-growth) features of the sPP lamellae. This analysis is further supported by the "straight" growth of lamellae beyond the substrate crystal limit, where the influence of 3Ph or 4Ph is limited. To summarize, we associate "straight" sPP lamellar morphology with "simple" epitaxial

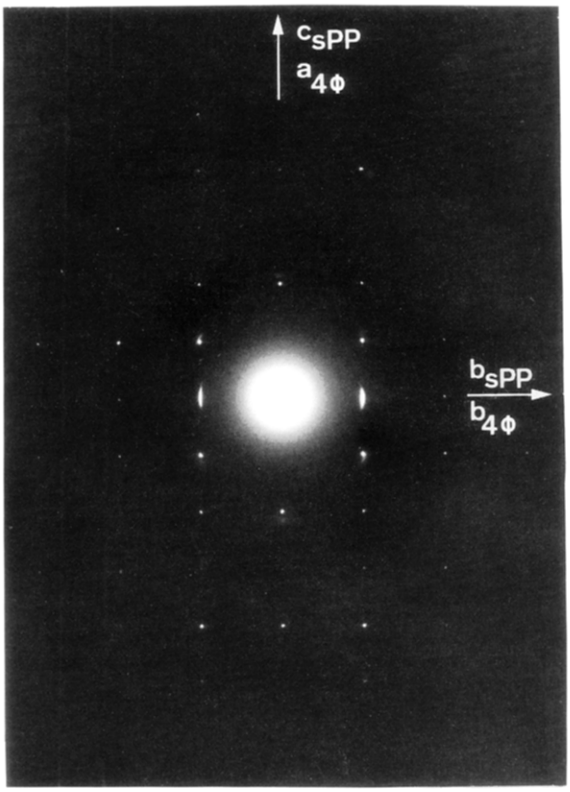


**Figure 5.** Composite electron diffraction pattern of a *p*-quaterphenyl substrate crystal (sharp diffraction spots) and of the sPP film epitaxially crystallized on this substrate (arced reflections), with the respective orientations indicated.

crystallization of sPP from the melt and take "corrugated" lamellar morphology as an indicator of local eutectic crystallization, i.e. of initial local dissolution of the substrate in molten sPP prior to crystallization.

*The sPP/substrate epitaxial relationship* can easily be established by electron diffraction since 3Ph or, better, 4Ph (due to its higher melting temperature, i.e. 320 °C versus 210 °C) sublimes only slowly in the electron microscope vacuum. When 4Ph is not dissolved prior to EM and ED examination, composite polymer–substrate electron diffraction patterns can be recorded, as illustrated in Figure 5, in which sharp spots correspond to 4Ph and broader arcs to sPP.

The 4Ph diffraction pattern can be indexed on the basis of an $a^*b^*$ reciprocal net of dimensions 0.805 and 0.555 $nm^{-1}$, which confirms that the large substrate surface is (001). Note that 3Ph yields essentially similar results, since linear polyphenyls are isomorphous in this contact plane, the different unit cells differing only by the length of the *c* axis (parallel to the molecular axis), which is incremented by ~0.41 nm for each additional phenyl ring.[18]

Analysis of the sPP diffraction pattern (Figure 6) is equally straightforward: the crystal lattice of sPP is seen along the $a^*$ axis, as indicated by the 0.74 nm periodicity (*c* axis) and the presence of a prominent reflection of spacing 0.56 $nm^{-1}$, i.e. *b*/2. The epitaxial relationship is therefore

$$(100)_{sPP}//(001)_{4Ph\ or\ 3Ph} \quad \text{with}$$

$$c_{sPP}//a_{4Ph\ or\ 3Ph} \quad \text{and}$$

$$b_{sPP}//b_{4Ph\ or\ 3Ph}$$

The lattice matching is two-dimensional, and 4Ph and

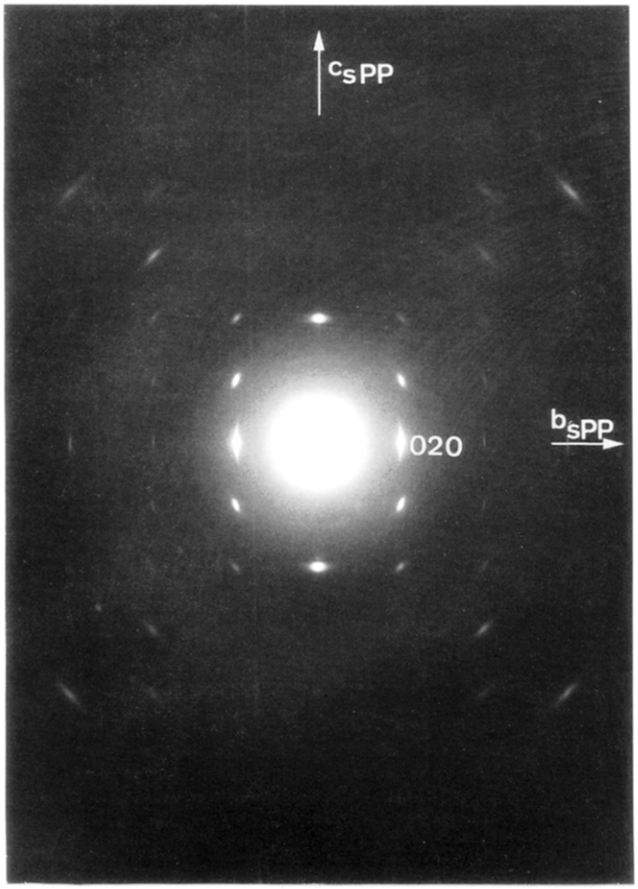


**Figure 6.** Electron diffraction pattern of an sPP film as in Figure 5 after removal of the substrate. Note the strong 020 reflection.

3Ph were actually selected on the basis of this anticipated lattice matching. Using room temperature crystallographic parameters, it amounts to (1) along the sPP chain direction

$$100\frac{c_{sPP} - a_{4Ph}}{a_{4Ph}} = \frac{0.74 - 0.805}{0.805} = -8.1\%$$

and (2) normal to the chain direction

$$100\frac{b/2_{sPP} - b_{4Ph}}{b_{4Ph}} = \frac{0.56 - 0.555}{0.555} = 0.9\%$$

*The details of the sPP crystal structure* need to be assessed in some depth. The $b$ axis parameter is clearly 1.12 nm, as revealed by the existence of a clear set of $01l$ and $03l$ reflections. These rows of reflections (best observed in tilted samples, as shown in Figure 7) would be absent were the $b$ parameter reduced to 0.56 nm (cell I of Corradini et al. or cell II, cf. Figure 1 of the companion paper). Doubling of the $b$ parameter and the very presence of the 020 reflections (seen in Figure 6 but forbidden for the C-centered cell I) both confirm a molecular packing as in cell III with *alternation of helical hand* along both $a$ and $b$ axes.

However, packing defects or $b/4$ shifts of whole layers (as discussed in the Introduction) do exist. They are most vividly illustrated when the epitaxial film is rotated about the $b$ axis (Figure 7) which brings prominent diffuse reflections into diffracting position. These are, seen in cross section, the diffuse streaks extending along $h11$ which are better and more fully imaged when single crystals are tilted around their $a$ axis.[4] Such streaks are produced in association with equatorial $h20$ streaks and reveal the existence of $b/4$ shifts of successive layers of chains.

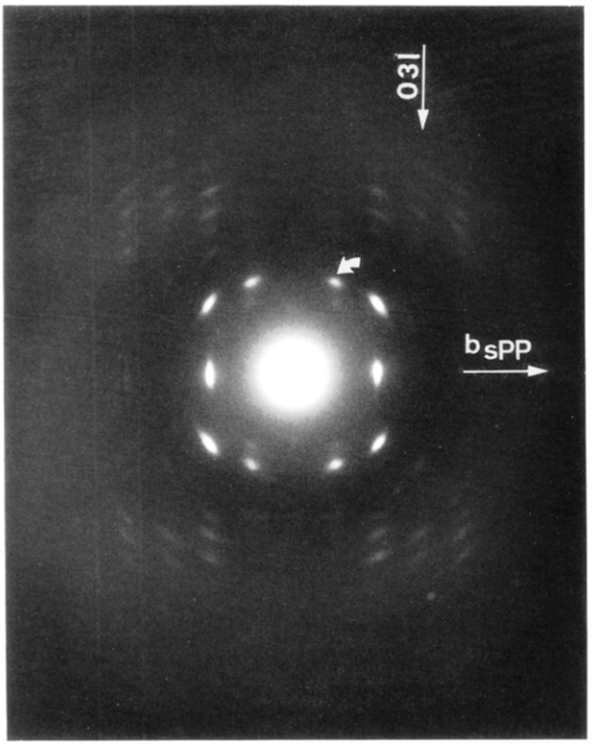


**Figure 7.** Diffraction pattern of an epitaxially crystallized sPP film as in Figure 6, but tilted around the $b$ (horizontal) axis. Note the appearance of $h11$ streaks seen in the cross section (curved arrow) and clear rows of $03l$ reflections (indicated).

To summarize, epitaxially crystallized sPP is essentially made of the so-called cell III structure which implies systematic alternation of helical hand along both $a$ and $b$ axes. Structural disorder exists mainly along the $b$ axis in the form of packing defects associated with interchain placement and helix chirality, as has been demonstrated for single crystals and bulk specimens.[4-6]

**2. Atomic Force Microscopy: Direct Visualization of Helical Hand.** AFM examination of epitaxially crystallized sPP at molecular resolution proved to be a technical challenge. The main difficulty appears to lie in the relative softness of the polymer film (which causes it to deteriorate rapidly when being probed) and/or in the excessive adhesion of the tip to the surface. As indicated in the Experimental Section, these difficulties could be overcome by using a "liquid cell" whereby we could probe the sample immersed in water.

Low-resolution micrographs of the epitaxially crystallized sPP films confirm the lamellar morphology observed by electron microscopy. Figure 8 shows an area with essentially parallel lamellae, as observed in parts of the bright field TEM pictures. The lamellar thickness appears at first sight quite variable, but closer examination reveals that the average thickness is ~15 nm. The variability results from tight packing of some lamellae which apparently blurs (but does not completely hide) interlamellar regions, whereas others are further apart: this morphology seems to reflect, on a more local scale, that illustrated in Figure 3.

Atomic scale resolution pictures of the sPP films have been obtained under both dry and wet conditions. Both results are presented here, as they illustrate pitfalls and improvements linked with these different imaging conditions. Figure 9a illustrates the best conventional AFM results obtained on "dry" sPP films. Imaging difficulties are evident. In particular, due to rapid deterioration of

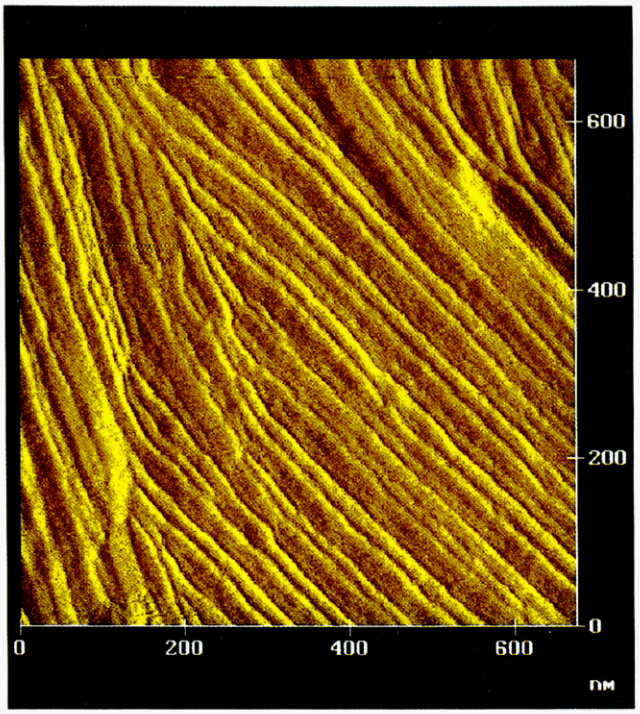


**Figure 8.** Lamellar morphology of an sPP film revealed by AFM. Imaging conditions: liquid cell; scan rate, 1 Hz or 8 min; constant height mode (force imaging); no filter.

the image, it proved impossible to reach atomic resolution simultaneously for right- and left-handed helices. As is well-known, AFM resolution is not equivalent in the $x$ (horizontal or scan) and $y$ (orthogonal) directions on the sample plane. In the scan direction, resolution is limited by a stick–slip process of the tip scanning the sample surface,[19] whereas better resolution in the orthogonal direction is dependent on the density of scan lines.

Since helices of opposite hand display molecular features at right angles to each other on the sPP surface of the epitaxially crystallized samples, the scanning direction should be parallel to either $b$ or $c$ axes in order to reveal equally helices of both hands. Under these conditions, we invariably obtained insufficient resolution to allow clear visualization of either hand. However, scanning in any other orientation made it possible to visualize helices of one hand only, at the expense of a worsened resolution for their antichiral counterparts. This is the type of image shown in Figure 9a, with the power spectrum (Figure 9b) and Fourier-filtered image (Figure 9c). As can be expected from the very crude transform, with only five pairs of exploitable spots and the smallest spacing of 3.5 $Å^{-1}$, resolution of the filtered picture is poor. It shows nevertheless a nearly rectangular pattern with dimensions 1.0 nm × 0.7 nm, consistent with the sPP crystal structure (in this set of experiments, the calibration of distances in our AFM was underevaluated by about 10%). The $n$-pentane groups are not clearly resolved, but elongated features (visible in the upper right part of Figure 9c) at 45° to the chain axis (nearly parallel to the lamellar normal and known, from low-resolution pictures, to be oriented at one o'clock) may correspond to the set of $CH_3$, $CH_2$, and $CH_3$ units of the sPP helix: on this basis, only left-handed helices, ≈1 nm apart, are "imaged" in Figure 9c, confirming directly the doubled unit cell along $b$.

Improvement in both resolution and stability of the picture are very substantial when the film immersed in water is probed. Parts a–c of Figure 10 illustrate one out of several sets of comparable images obtained in this study. They show (Figure 10a) the unfiltered image taken from an area located near the center right of Figure 8, the Fourier transform (Figure 10b) of the best resolved, upper left part of Figure 10a, and the corresponding Fourier-filtered image (Figure 10c). Improvement in resolution is readily apparent, since the unfiltered image already reveals the two helical hands. The power spectrum (Figure 10b) is unusually rich, as about *20 pairs* of spots are now available for image reconstruction. The outermost spots (at eight o'clock) correspond to spacings of 1.7 $Å^{-1}$, which indicates that methyl group resolution has been reached. This is indeed confirmed in many parts of Figure 10c in which the $CH_3$, $CH_2$, and $CH_3$ substructure of the elongated features is discernible. Again, since the scanning direction is not parallel to an axis of symmetry of the sPP lattice, resolution is better for one helical hand. Here again, the chain axis is oriented at about one o'clock, and left-handed helices are better resolved than right-handed ones. Beyond these relatively minor details, parts a and c of Figure 10 reveal a crystal structure made of alternating right- and left-handed helices with the $c/2$ shifts expected from a cell with space group *Ibca*, as illustrated in Figure 10d.

## Discussion

Whereas AFM recognition of the helical hand of large helices (e.g. double-stranded DNA) is now nearing routine work, the task is more difficult for synthetic polymers since (a) helices are not stabilized by strong intrachain (or interstrand for DNA) forces but only by weak intermolecular forces, and can thus be imaged only when embedded in their crystallographic surroundings, and (b) geometrical and structural factors (size of the helix, existence of side chains, up or down orientation, etc.) may blur or altogether hide the underlying helical hand.

A number of AFM observations on flat, crystalline surfaces with the chain axis in the surface plane have been reported. For obvious reasons of resolution, AFM of helical polymers *bearing no side chains* has not yet achieved recognition of helix hand. For PTFE, the helical shape (a gentle $13_6$ or $15_7$ helix) is nearly cylindrical, and helical hand could not be recognized from existing pictures although some elements of the helix substructure have indeed been imaged.[10,11]

Polymer helices bearing bulkier side chains are a priori more favorable candidates in view of their larger diameters and the fact that the helical path is prominently displayed by the side chains. An additional *crystallographic* feature may contribute to facilitate observation of the helical hand, as best illustrated with polyolefins crystallizing in the hexagonal space group $R3c$ or $R\bar{3}c$. These space groups are characterized by full layers of isochiral chains, successive layers being antichiral. If such layers can be exposed and imaged by AFM, the side chains may create a linear pattern oblique to the helix axis and allow recognition of the *common* helical hand (in contrast to the individual hand as in the present study). Snétivy et al.[14a] have observed such an oblique pattern in stretched thin films of $\alpha$ phase isotactic polypropylene ($\alpha$ iPP). This phase has a monoclinic unit cell but is based on the above alternation of layers of helices. The exposed plane is (110) which includes helices of both hands, but seen from a different viewing angle: the oblique pattern reflects more prominently the mutual arrangement of their side chains than the side chains of individual helices. Nevertheless, Snétivy and Vancso[14b] appear to have resolved—in filtered images—the hand of such individual helices.

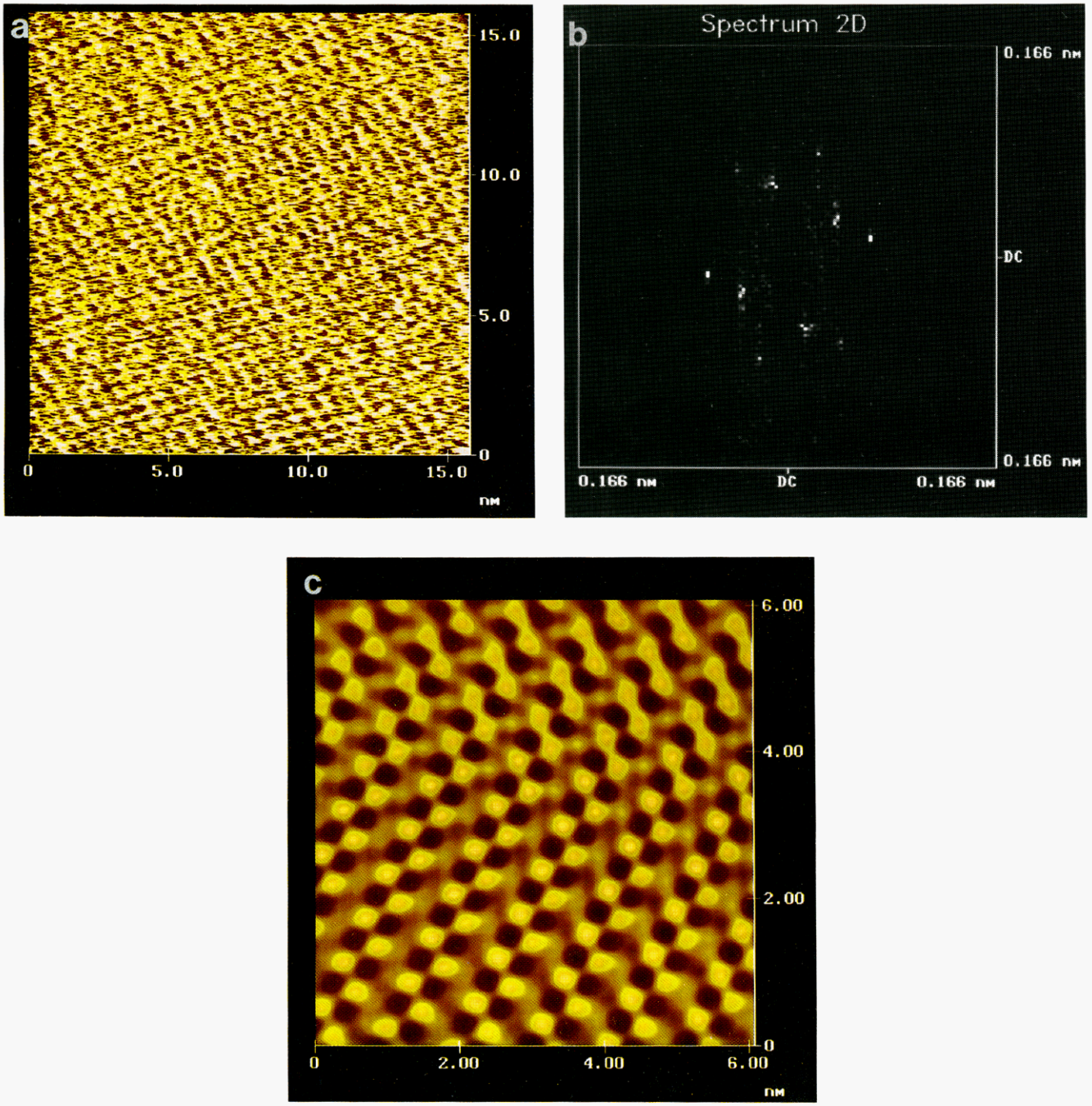


**Figure 9.** (a) AFM picture of the contact face of sPP. Imaging conditions: force imaging (constant height) in air; no filter; scan rate, 57 Hz or 8 s. (b) Power spectrum of (a). (c) Fourier-filtered image of (a) using the five pairs of spots visible in (b).

Exposure of the required crystallographic contact plane does not protect from yet another possible pitfall, which was indeed encountered in a recent AFM investigation of the contact faces of $\alpha$ and $\gamma$ phase iPP epitaxially crystallized on organic substrates (nicotinic or benzoic acid).[13] Given the setting of the 3-fold helices in the layer, two structurally different contact faces may exist: one in which two methyl groups are exposed on the contact face (and which is ideally suited to reveal the oblique pattern of methyl side chains) and one in which only one methyl side chain per unit cell is exposed, in which case it would normally not be possible to determine the hand of the underlying helix. It turned out unfortunately that the latter face is the actual contact face. The hand was nevertheless deduced in an *indirect* way from the relative $c$ axis shift of neighboring helices, i.e. by analysis of the $a$ axis dip (monoclinic $\beta$ angle) in the exposed $ac$ face: this dip differs when layers of right- or left-handed helices are exposed, and therefore offers a means to discriminate the helical hand.

In sharp contrast to the above limitations, sPP provides an unusual opportunity for *direct* observation of helical hand as a result of a highly favorable *molecular conformation*. Contrary to most helical structures where isoconformation of residues prevails, successive side chains in sPP have *opposite dips* relative to the helical axis. In the $bc$ contact plane imaged in this investigation, these dips parallel the helical path; i.e. *the side chain organization highlights the helical path* and produces a pseudoparaffinic molecular segment of sufficient size. Further, since the $CH_3$, $CH_2$, and $CH_3$ groups are all in the same $bc$ plane (i.e. have identical $x/a$ coordinates), they are at the same

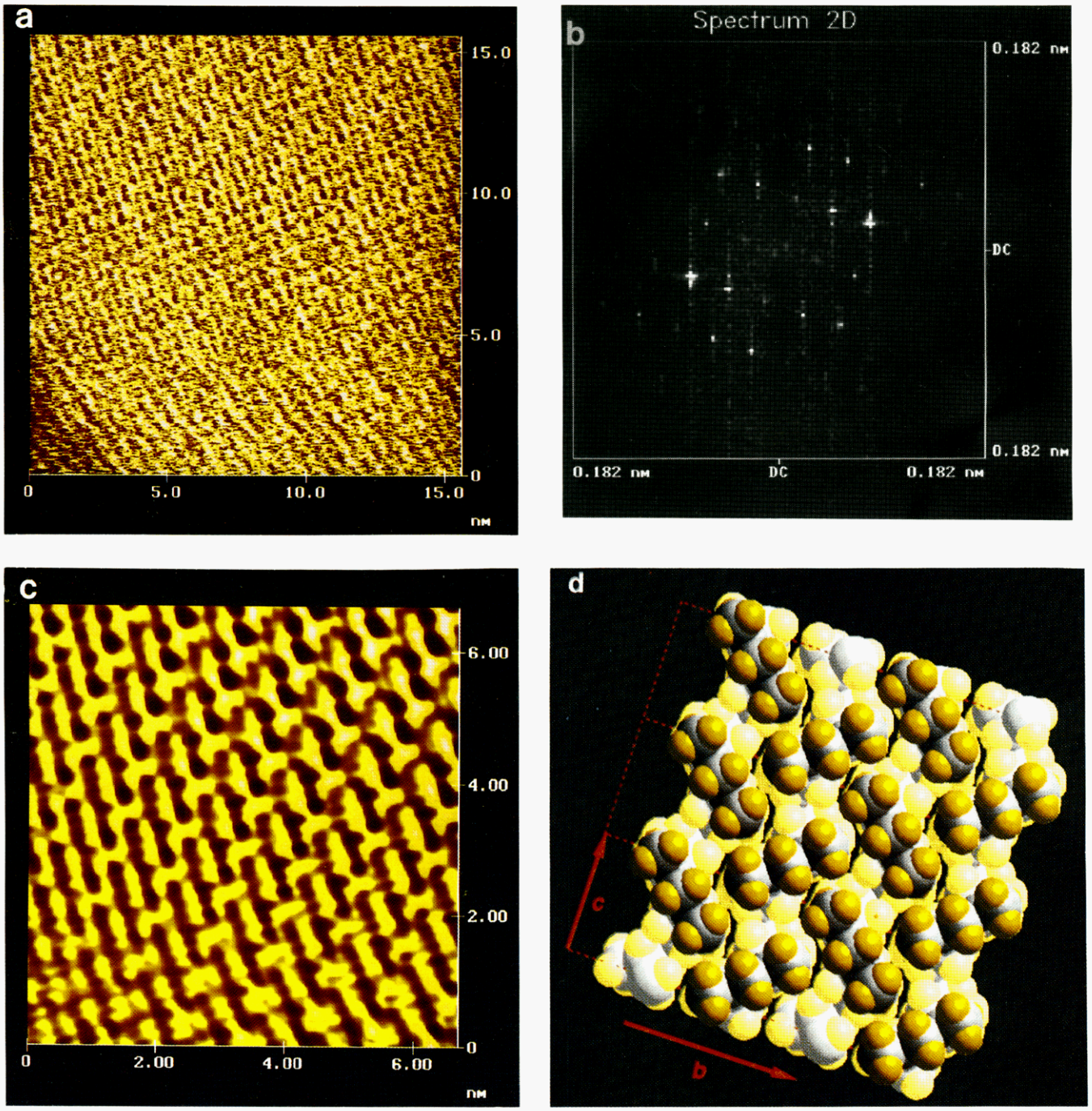


**Figure 10.** (a) High-resolution AFM image of an area near the center of Figure 8, recorded in the liquid cell (force imaging, constant height mode, no filter, scan rate 57 Hz or 8 s). Orientation of chain axes: at ≈1 o'clock. (b) Power spectrum of the upper left part of the picture in (a). Periodicities along and normal to the chain axis direction are 0.72 and 1.1 nm, respectively. Note the appearance of more intensity peaks than in the electron diffracton pattern of Figure 6, linked with the fact that the surface symmetry of sPP differs from its bulk one. (c) Fourier-filtered image of the upper part of (a) produced when selecting 20 pairs of spots in the power spectrum in (b). Note the better resolution of $CH_3$, $CH_2$, and $CH_3$ units oriented nearly normal to the scan direction. (d) Schematic representation of the AFM image in (c) using molecular modeling and shown in correct mutual orientation (cell III of Figure 1, space group *Ibca*). The atomic van der Waals radii are depicted at 83% of their values to allow better visualization of the individual chains; the uppermost groups visualized in AFM are darkened.

AFM imaging level and therefore easier to observe. Taken together these two features permit recognition of the *individual* (as opposed to *common*; cf. the above iPP case) helical hand, as well as observation of arrays of helical hands, i.e. of the *mutual* arrangement of right and left hands in this specific crystallographic plane.

The present investigation is not, however, free of crystallographic constraints on the nature of the plane to be imaged. Indeed, it suffices to note that were the other lateral face (i.e. the *ac* plane) the exposed surface, AFM would *not* have been able to detect the helical hand: on that face, the methyl side chains have the *same* $z/c$ coordinates (cf. Figure 2), and right- and left-handed helices would be indistinguishable on the basis of their surface features (methyl groups). This observation further underlines the exceptional usefulness of epitaxial crystallization, which (a) helps to select specific contact faces of crystalline polymers, (b) ensures a constant structural pattern linked with repetition of locally favorable epitaxial interactions over the entire contact surface, and (c) on a

more experimental side, delivers a polymer surface nearly molecularly flat since it reflects the initial crystal habit of the organic substrate.

The AFM results shown in Figure 10a,c confirm directly in *real space* the striking regularity of the helical hand alternation characteristic of space group *Ibca*. Moreover, as already indicated in the Introduction, sPP was selected, not only for its suitability for helical hand determination but also for its potential to reveal and study *local crystallographic defects*. The streaks observed in the diffraction pattern (cf. Figure 7) do indicate shifts of $b/4$ of individual *bc* layers, portions of layers, or groups of layers[4,6] but give limited clues about the nature of the defect(s) from which they emanate. If such shifts affect full individual layers, they would not be noticeable by AFM since only one layer (actually the outermost one) is imaged. If, however, multiple nucleation takes place in any given exposed *bc* layer, vacancies with $b/4$ dimensions should be created, which are susceptible to be imaged by AFM. Additionally, occasional close packing of isochiral helices in the *bc* plane (as in cell I) appears as a possible defect feature supported by packing energy calculations,[20] by observation of homoepitaxy (cf. companion paper), and by a characteristic splitting of $CH_3$ bands in the NMR spectra.[21] This close packing of isochiral helices is in principle also accessible to AFM imaging.

At this stage, we have been unable to identify with certainty either any point vacancies or any isochiral defects in our AFM images. As suggested by recent molecular and lattice modeling of a variety of possible defective structures,[4] such defects should be very rare, even in samples crystallized at low $T_c$. Further, for $b/4$ point vacancies, it is likely that they are mobile within the lattice and are annihilated by movement of chains (or groups of chains) along $b$ in $(2n)b/4$ increments.[4] Since epitaxial crystallization on an active substrate does not allow low-$T_c$ crystallization, the probability of forming any such defects is even further reduced in the present specimens. For this reason, additional work is in progress in an attempt to localize and discover such chirality-related crystallographic defects. Judging from present results, their direct observation is now within reach of the AFM technique.

## Conclusions

Epitaxial crystallization of sPP thin films on linear oligophenyl substrates makes it possible to expose the crystallographic *bc* contact face of this polymer. Electron microscopic and diffraction investigations confirm that the crystal structure involves full antichiral packing of neighboring helices, as in the cell III proposed recently. We showed that epitaxially crystallized sPP films are highly suitable for AFM probing of the hand of *individual helices* exposed in the contact face. This is so because the organization of side chains highlights the helical path and creates an extended pseudo *n*-pentane segment oblique to the helix axis and of sufficient size for AFM resolution. AFM performed in a liquid cell does indeed reveal both right and left helix hands, which are found to alternate regularly in the contact plane, in agreement with the recent *Ibca* space group assignment. Further work should help observe various rare local structural features associated with packing-related crystallographic defects.

**Acknowledgment.** W.S. acknowledges support from the Université Louis Pasteur, Strasbourg, and the Centre National de la Recherche Scientifique. This work has been funded in part by a research grant from Exxon Chemical International to the Institut C. Sadron and to M.S.

## References and Notes

(1) Corradini, P.; Natta, G.; Ganis, P.; Temussi, P. A. *J. Polym. Sci., Part C: Polym. Lett.* **1967**, *16*, 2477.
(2) Lotz, B.; Lovinger, A. J.; Cais, R. E. *Macromolecules* **1988**, *21*, 2375.
(3) Lovinger, A. J.; Davis, D.; Lotz, B. *Macromolecules* **1991**, *24*, 552.
(4) Lovinger, A. J.; Lotz, B.; Davis, D.; Padden, F. J., Jr. *Macromolecules* **1993**, *26*, 3494.
(5) De Rosa, C.; Corradini, P. *Macromolecules* **1993**, *26*, 5711.
(6) Auriemma, F.; De Rosa, C.; Corradini, P. *Macromolecules* **1993**, *26*, 5719.
(7) Stocker, W.; Bar, G.; Kunz, M.; Möller, M.; Magonov, S. N.; Cantow, H.-J. *Polym. Bull.* **1991**, *26*, 215.
(8) Hansma, H.; Motademi, F.; Smith, P.; Hansma, P.; Wittmann, J. C. *Polymer* **1992**, *33*, 647.
(9) Magonov, S. N.; Cantow, H. J. *J. Appl. Polym. Sci., Appl. Polym. Symp.* **1992**, *51*, 3.
(10) Dietz, P.; Hansma, P. K.; Ihn, K. J.; Motamedi, F.; Smith, P. *J. Mater. Sci.* **1993**, *28*, 1372.
(11) Brouwer, H.-J. Undergraduate Thesis, University of Groningen, 1992.
(12) Snetivy, D.; Vancso, G. J. *Macromolecules* **1992**, *25*, 3320.
(13) Stocker, W.; Magonov, S. N.; Cantow, H. J.; Wittmann, J. C.; Lotz, B. *Macromolecules* **1993**, *26*, 5915.
(14) (a) Snětivy, D.; Guillet, J. E.; Vancso, G. J. *Polymer* **1993**, *34*, 429. (b) Snětivy, D.; Vancso, G. J. *Polymer* **1994**, *35*, 461.
(15) Schumacher, M.; Lovinger, A. J.; Agarwal, P.; Wittmann, J. C.; Lotz, B. *Macromolecules*, following article in this issue.
(16) Wittmann, J. C.; Lotz, B. *Prog. Polym. Sci.* **1990**, *15*, 909.
(17) Drake, B.; Prater, C. B.; Weisenhorn, A. L.; Gould, S. A. C.; Albrecht, T. R.; Quate, C. F.; Cannell, D. S.; Hansma, H. G.; Hansma, P. K. *Science* **1989**, *243*, 1586.
(18) Wittmann, J. C.; Lotz, B. *J. Polym. Sci., Polym. Phys. Ed.* **1981**, *19*, 1837.
(19) Fujisawa, S.; Sugawara, Y.; Ito, S.; Mishima, S.; Okada, T.; Morita, S. *Nanotechnology* **1993**, *4*, 138.
(20) Corradini, P.; Pirozzi, B.; Napolitano, R. *Atti Accad. Naz. Lincei, Cl. Sci. Fis., Mat. Nat., Rend.* **1991**, *2*, 341.
(21) Sozzani, P.; Simonutti, R.; Galimberti, M. *Macromolecules* **1993**, *26*, 5782.